Multinuclear Solid-State NMR, Self-Diffusion Coefficients, Differential Scanning Calorimetry, and Ionic Conductivity of Solid Organic−Inorganic Hybrid Electrolytes Based on PPG−PEG−PPG Diamine, Siloxane, and Lithium Perchlorate

Hsien-Ming Kao,* Shih-Wei Chao, and Pai-Ching Chang

Department of Chemistry, National Central University, Chung-Li, Taiwan 32054, ROC

Received July 15, 2005; Revised Manuscript Received December 8, 2005

ABSTRACT: Organic−inorganic hybrid electrolytes based on poly(propylene glycol)-*block*-poly(ethylene glycol)-*block*-poly(propylene glycol) bis(2-aminopropyl ether) (D2000) complexed with $LiClO_4$ via the co-condensation of an epoxy trialkoxysilane and tetraethoxysilane have been prepared and characterized. The hybrid electrolytes thus obtained were rubbery thin films with good mechanical strength and a good degree of elasticity. Characterization was made by a variety of techniques including alternating current impedance, Fourier transform infrared spectroscopy, differential scanning calorimetry (DSC), multinuclear solid-state NMR spectroscopy, and pulse-gradient spin−echo (PGSE) NMR measurements. A VTF (Vogel−Tamman−Fulcher)-like temperature dependence of ionic conductivity was observed for all the compositions studied, implying that the diffusion of charge carriers was assisted by the segmental motions of the polymer chains. A maximum ionic conductivity value of 6.23×10^{-5} S/cm was obtained at 30 °C. ^{13}C cross-polarization/magic angle spinning NMR results from variable contact time measurements along with 2D wide-line separation NMR indicated that a significant decrease in the mobility of the polymer chains as the salt content was increased, consistent with the increase in T_g as observed by DSC. Solid-state ^7Li NMR characterization was performed to study ionic mobility by measuring spectral line widths, T_1 relaxation times, and diffusion coefficients. The results of the lithium diffusion coefficient measurements indicated that the ionic conductivity in the present electrolytes was mainly dominated by the mobility of the lithium cations.

Introduction

Development of highly conductive solid polymer electrolytes (SPEs) has proceeded for practical use in lithium-ion battery systems due to advantages such as safety, mechanical properties, high-energy density, and ease of fabrication of thin films of desired sizes as compared with those with liquid electrolytes.[1−3] Due to the solvation power and complexing ability of poly(ethylene oxide) (PEO) to alkali metal ions, many studies on SPEs have dealt with the systems consisting of polyether-like structure with a wide variety of lithium salts. However, the practical use for PEO-based electrolytes is often hindered due to their low conductivity at room temperature ($\sim 10^{-7}-10^{-8}$ S/cm) and poor mechanical properties. Ion conduction in solid polymer electrolyte systems is generally dependent on the segmental mobility of the solvating polymer chains and takes place predominantly in the amorphous phase rather than crystalline phases,[3,4] although the ion transport associated with the crystalline phase can yield a significant contribution to the conductivity under appropriate circumstances, including alignment of the polyether helices.[5−8] While PEO chains act as solvents for lithium salts, PEO-based electrolytes are prone to crystallization. Therefore, it requires a better understanding of the ion transport mechanism in order to have significant improvement in conductivity for SPEs.

To alleviate the limitations of polyether-based electrolytes, considerable advance has been gained by designing new polymer electrolytes based on organic−inorganic hybrids or nanocomposite systems, which combine high mechanical strength with high ionic conductivity needed for application in solid-state lithium polymer batteries.[9−27] Composite polymer electrolytes (CPEs), obtained by dispersing inorganic particles, such as nanosized TiO_2,[9−11] silica,[12−14] and alumina,[10] as the fillers in the polymer electrolytes, generally exhibit sufficient mechanical strength, higher ionic conductivity, and better lithium anode and electrolyte interfacial stability. Alternatively, a variety of organic−inorganic hybrids comprising covalent bonds or only weak physical bonds between the inorganic (siloxane) and organic (polymer) phases have been proposed.[15−27] For example, Mello et al.[15] reported two novel families of hybrid electrolytes with remarkable conductivities at room temperature, which differ essentially in the type of bond connecting the inorganic and organic phases. The introduction of a silicate network into the polymer matrix provides simultaneously an amorphous structure and good thermal, mechanical, and chemical stability. Therefore, these hybrid polymer electrolytes, so-called *ormolytes* (*or*ganically *mo*dified electro*lytes*) are very promising to overcome the disadvantages associated with conventional SPEs.

A simple method for obtaining organic−inorganic hybrids is mixing an organic polymer with a silicon alkoxide such as tetraethoxysilane (TEOS), followed by a sol−gel reaction involving the hydrolysis and polycondensation of TEOS. However, the incompatibility of the two components of the polymer/silica hybrids makes the dispersion of the inorganic particles into the polymer matrix difficult. This is obviously not a favorable factor in the preparation of transparent free-standing hybrid films due to phase separation, especially at high silica contents. Furthermore, the morphology and interfacial properties of the separated two phases will not lead to composites with excellent properties. Therefore, it is of great importance to improve the compatibility between the two phases for the preparation of organic−inorganic hybrids with good

* Corresponding author. Telephone: +886-4275054. Fax: +886-4227664. E-mail: hmkao@cc.ncu.edu.tw.

10.1021/ma051550q CCC: $33.50
Published on Web 01/07/2006

properties. The use of functionalized alkoxysilanes that can blend with the polymer matrix not only improves the miscibility between the organic and inorganic entities but also guarantees the amorphous behavior of the hybrid electrolytes.

Among the several techniques employed, solid-state NMR has emerged as one of the highly sophisticated techniques to obtain the information about the local environment and the mobility of the charge carriers and also to gain insights into the polymer−salt interactions in the polymer electrolytes.[28−36] A great advantage of NMR technique is its sensitivity to the dynamics of the lithium ions and the polymer chains based on the NMR relaxation times, depending on the time modulation of the local interactions (e.g., chemical shielding, dipolar, quadrupolar), which indirectly reflects the motions of the nucleus. Measurements of these relaxation times as a function of temperature have been widely used to study the correlation between the mobility of the charge carriers and the polymer chains in SPEs.

In contrast to NMR relaxation times such as T_1 and T_2, the pulse-gradient spin−echo (PGSE) NMR provides a direct measurement of the translational self-diffusion coefficients.[37,38] PGSE NMR methods offer the opportunity to obtain quantitative measurements of ionic diffusion coefficients to compare with measurements of ionic conductivity and hence gain understanding of the degree of ionic association and its variation with salt concentration and temperature. However, most of the PGSE NMR studies have been focused on plasticized polymer electrolytes. Relatively few studies have been reported for solid polymer electrolyte systems due, in part, to the high power requirement of PGSE methods.[39−42]

In the present work, a new organic−inorganic hybrid electrolyte based on $H_2N-PPG_{40}-PEG_5-PPG_{40}-NH_2$ triblock copolymer (Jeffamine, D2000, $M_w = 2000$), where PPG and PEG represent poly(propylene glycol) and poly(ethylene glycol), respectively, through the co-condensation with (3-glydicyloxypropyl)trimethoxysilane (GLYMO) and TEOS as the silica sources was prepared. Since the ethylene oxide and propylene oxide units of D2000 are short, the mechanical property of D2000-based polymer electrolyte is a major concern for its practical applications. The coupling agent, GLYMO, was chosen to improve the compatibility between organic and inorganic phases. It is anticipated that the functionality, i.e., the epoxy ring, in the GLYMO can provide a cross-linking center to interact with the amine end groups of D2000 triblock copolymer to generate a nanocomposite film comprising silicate networks. The in-situ built-in inorganic phase, formed by the condensation of TEOS and GLYMO, results in reinforcement of the rubbery network and thereby improves the mechanical properties of the hybrid materials. The present work emphasizes the relationships between the structure and transport properties of these materials in order to gain more insights into the role for ion−polymer/ion−ion interactions, the nature of the charge carrier, and the ionic association process in the ionic conductivity. Multinuclear (^{13}C, ^{29}Si, and ^{7}Li) solid-state NMR techniques were used to study the microscopic structure of the hybrid materials and the mobility and the local environments of the lithium cations involved in these systems. We also present the measurements of Li^+ diffusion coefficients, a parameter directly related to ionic conductivity, for the present hybrid electrolytes using PGSE NMR techniques. The temperature dependence of the ^{7}Li diffusion coefficient was used to elucidate the relationships between Li^+ diffusivity, phase behavior, and ionic conductivity.

Experimental Section

Preparation of Hybrid Electrolyte Films. The starting materials $LiClO_4$ and D2000 (both from Aldrich) were dried at 120 °C for 24 h and at 50 °C for 12 h under vacuum ($<10^{-3}$ Torr) prior to their use, respectively. GLYMO (Fluka) and TEOS (Aldrich) were used as received. Synthesis of the organic−inorganic hybrid electrolyte based on D2000 was carried out via a sol−gel route. In a typical synthesis, 0.2 or 0.4 g of TEOS was first mixed with GLYMO in a molar ratio of 1:4 and then hydrolyzed with 0.5 mL of 2 M HCl at room temperature for 1 h. In another solution, 5.0 g of D2000 dissolved in 60 mL of acetonitrile was mixed with $LiClO_4$ to achieve the desired [O]/[Li] ratios and was stirred for 1 h. These two solutions were then mixed at room temperature for 24 h under constant stirring. The casting solution was put into Telfon dishes, and the solvent was slowly evaporated at room temperature for 24 h. Afterward, the materials were heated at 95 °C under vacuum for another 24 h to give a piece of transparent and crack-free film. The materials thus obtained are rubbery thin films with good mechanical strength and a good degree of elasticity. The salt concentrations were expressed as the ratio of the total concentration of PEG and PPG ether oxygens to the lithium ion concentration, i.e., the [O]/[Li] ratio. The hybrid electrolyte materials were labeled as $x-y-$D2000, where x represents the weight of TEOS relative to the weight of D2000 (5 g), either 0.2 or 0.4, and y represents the [O]/[Li] ratio. The films were then stored in a glovebox under a nitrogen atmosphere for further measurements. The thickness of the films was controlled to be in the range of 150−200 μm.

DSC Thermograms. Differential scanning calorimetry (DSC) studies were performed in the temperature range of −60−125 °C using a Mettler Toledo DSC system at a heating rate of 5 °C/min. The sample weights were maintained in the range of 5−6 mg, and all experiments were carried out under a nitrogen flow. The glass transition (T_g) and melting transition temperatures (T_m) were measured, and the associated enthalpy changes (ΔH_f) were calculated. Glass transition temperatures were reported as the midpoint of the transition process.

FTIR Spectroscopy. FTIR spectra were obtained from a Bio-Rad FTS155 spectrometer at a resolution of 4 cm^{-1} using the KBr wafer technique. Band deconvolution of the resulting spectra was conducted to obtain the best fit for the band envelope.

AC Impedance Measurements. Alternating current (AC) impedance measurements of the hybrid electrolytes were performed using a CH Instrument Model 604A electrochemical analyzer over a frequency range of 10 Hz to 100 kHz with an amplitude of 10 mV. All the specimens were sandwiched by two polished stainless steel blocking electrodes for conductivity tests. These measurements were performed in the temperature range of −25 to +65 °C, and the system was thermally equilibrated at each selected temperature for at least 1 h. The conductivity values (σ) have been calculated from the equation $\sigma = (1/R_b)(t/A)$, where R_b is the bulk resistance, t is the thickness, and A is the area of the sample.

Solid-State NMR Measurements. Solid-state NMR experiments were performed on a Varian Infinityplus-500 NMR spectrometer, equipped with a Chemagnetics 7.5 mm magic angle spinning (MAS) probe and a double-tuned wide-line probe. The Larmor frequencies for ^{7}Li, ^{13}C, and ^{29}Si nuclei are, respectively, 194.3, 125.7, and 99.3 MHz. MAS of the samples in the range of 3−5 kHz was employed for obtaining ^{13}C and ^{29}Si NMR spectra and some ^{7}Li NMR spectra. The Hartmann−Hahn condition for $^{1}H \rightarrow {}^{13}C$ cross-polarization (CP) experiments was determined using admantane. A $\pi/6$ excitation pulse of 2 μs and a recycle delay of 200 s were used to obtain ^{29}Si MAS NMR spectra. The ^{13}C and ^{29}Si chemical shifts were externally referenced to tetramethylsilane (TMS) at 0 ppm. The $^{1}H \rightarrow {}^{13}C$ CP/ MAS NMR spectra were also recorded as a function of contact time ranging from 0.2 to 18 ms. ^{7}Li NMR spectra were acquired under various conditions, either static or MAS with and without proton decoupling during the acquisition. The ^{7}Li line widths from the static measurements were taken to be the full width at half-height (fwhh) of the peaks and measured as a

function of temperature from −140 to +80 °C. ^{7}Li spin−lattice relaxation (T_1) measurements were conducted using an inversion recovery method (180°−τ−90°). Variable-temperature ^{7}Li{^{1}H} (i.e., proton-decoupled) MAS NMR spectra was acquired to reveal different local environments of the lithium cations. ^{7}Li chemical shifts were externally referenced to a 1 M aqueous solution of LiCl at 0 ppm.

2D ^{1}H−^{13}C WISE Experiments. ^{1}H wide-line spectra were acquired with the use of the 2D WISE (two-dimensional WIdeline SEparation spectroscopy) NMR pulse sequence developed by Schmidt-Rohr et al.[43] In the 2D WISE experiments, the proton magnetization evolves under the influence of dipolar coupling during the time t_1, and the ^{13}C signal is detected under MAS conditions during the time t_2. The experiment reveals proton wide-line spectra from the proton of the polymer chains along the ω_1 dimension, resolved by the ^{13}C chemical shifts of the polymer chains along the ω_2 dimension. Therefore, a correlation can be made between the chemical structure and segmental mobility of the polymer. Spectral widths of 40 and 100 kHz were used for the ω_2 and ω_1 dimensions, respectively. Typically, 128 t_1 increments were used in the 2D WISE experiments.

^{7}Li Diffusion Constant Measurements. The ^{7}Li diffusion coefficients were determined by PGSE NMR experiments. The PGSE NMR experiments were performed using a Doty 5 mm dual broadband gradient probe and a current amplifier provided by Varian. The PGSE pulse sequence starts with a 90° pulse followed by two identical gradient pulses, separated by a 180° pulse, which causes the echo to be attenuated when there are diffusing nuclei. The echo attenuation is related to the diffusion coefficient, D, and the parameters of the sequence according to the Stejskal−Tanner equation:[37]

$$I = I_0 \exp[-\gamma^2\delta^2 g^2(\Delta - \delta/3)D] \quad (1)$$

I is the echo amplitude obtained with application of the gradient pulses, and I_0 is the amplitude without gradient, γ is the gyromagnetic ratio of the observed nuclei, δ is the width of the gradient pulse, g is the magnetic field gradient amplitude, and Δ is the time interval between the leading edges of the gradient pulses. For each PGSE experiment, the gradient strength was varied by keeping all other parameters constant. Plots of $\ln(I/I_0)$ against $\gamma^2\delta^2 g^2(\Delta - \delta/3)$ give a straight line with a slope of $-D$. Therefore, the D value can be determined from the slope. Measurements were carried out on about 500 mg samples, which were loaded and packed into 5-mm Pyrex tubes in a very low humidity (<1 ppm) glovebox. The Pyrex tubes were flame-sealed under vacuum to prevent any contamination from outside air and moisture. The gradient strength was calibrated using the known self-diffusion coefficient of H_2O at 25 °C (2.23×10^{-5} cm^2/s).[44] In all cases the echo signal attenuation, I, versus the square of the gradient duration was well-described by a single exponential which is consistent with free diffusion. The self-diffusion coefficients were obtained in the temperature range of 30−120 °C. The typical reproducibility of the diffusion coefficient measurements is about ±3%.

Results and Discussion

DSC. Because the segmental mobility of the polymer chains is directly related to the mechanical and conductivity performance of polymer electrolytes, the glass transition temperature, T_g, of the electrolyte composition is a parameter which provides information which is useful in understanding the behavior of electrolyte systems. The thermal behavior of the cross-linked epoxy−siloxane polymer networks undoped and doped with $LiClO_4$ was measured using DSC, as shown in Figure 1. The DSC results of the samples studied are also summarized in Table 1. The T_g of pure D2000 copolymer is around −59.5 °C. For a given silica content, the T_g value in general increases with increasing lithium contents, suggesting the formation of transient cross-links between the salt and the polyether phase. This effect decreases segmental motion of the polymer chains and thus increases the T_g. The effects of silica contents on the T_g values of D2000 can be directly compared for the samples without the lithium salt doping. Without the lithium salt doping, there is a gradual increase in T_g, from −59.5 °C for pure D2000 to −55.1 °C for 0.4−∞−D2000, with increasing silica contents (see Table 1), indicating that the T_g value of D2000 is also dependent on the silica contents. For the hybrid electrolytes doped with both silica and lithium salt, the change in T_g on the addition of the silica filler was not so obvious at low lithium salt doping levels. At high salt doping levels, on the other hand, the T_g value increases significantly, for example, from −57.0 °C for 0.2−∞−D2000 (without lithium salt doping) to −38.4 °C for 0.2−16−D2000 ([O]/[Li] = 16). These results show that the mobility of the D2000, as measured by T_g, is predominantly affected by the high levels of lithium salt doping, but only slightly affected by the added silica.

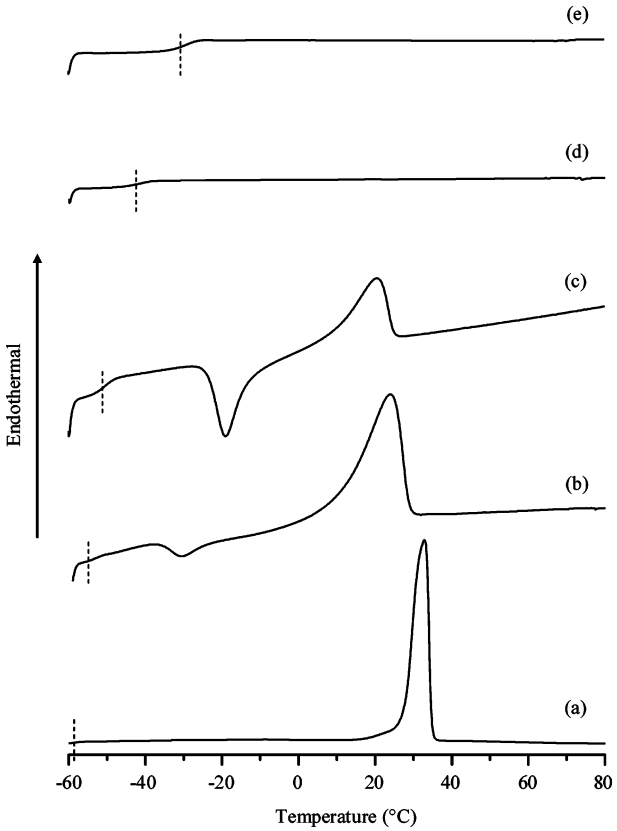

Figure 1. DSC thermograms of (a) pure D2000, (b) 0.4−32−D2000, (c) 0.4−24−D2000, (d) 0.4−16−D2000, and (e) 0.4−8−D2000. The T_g value is indicated by the dashed lines.

Table 1. DSC Results of the Hybrids Studied

sample	y, [O]/[Li]	T_g, °C	T_m, °C	ΔH_f, J/g	χ,[a] %
pure D2000	b	−59.5	32.8	113.0	100.0
0.2−y−D2000	b	−57.0	29.5	64.1	56.7
	32	−54.2	28.3	42.6	37.7
	24	−49.8	25.7	38.7	34.2
	16	−38.4	21.4	5.3	4.7
	8	−42.6			
0.4−y−D2000	b	−55.1	21.0	44.3	39.2
	32	−53.4	23.9	36. 9	32.6
	24	−50.6	20.6	23.1	20.4
	16	−40.8			
	8	−29.0			

[a] $\chi = \Delta H_f$(sample)/ΔH_f(pure D2000) × 100%. [b] No lithium salt was doped.

The T_m and the endothermic heat ΔH_f generally decrease and then disappear with increasing salt concentrations for both series of samples. This phenomenon indicates that the crystalline structure of D2000 is disrupted and that D2000 with Li^+ doping is gradually transformed into an amorphous form with the addition of $LiClO_4$. No clear melting transition is observable for the 0.2−8−D2000, 0.4−16−D2000, and 0.4−8−D2000 samples, indicating that the D2000 crystallization is successfully suppressed by the high levels of salt doping. Interestingly, the thermograms of the 0.2−16−D2000 and 0.2−24−D2000 samples exhibit exothermic peaks in the temperature range of −20 to −30 °C (Figure 1b,c), and endothermic peaks in the temperature range of 20−25 °C, corresponding to the recrystallization and the melting of D2000, respectively. For 0.4−*y*−D2000, the 0.4−24−D2000 and 0.4−32−D2000 samples also exhibit the same thermal behavior. No recrystallization exotherm is found in other hybrid electrolytes. Given the same [O]/[Li] ratio, the lack of T_m for 0.4−16−D2000, whose silica content is doubled as compared to 0.2−16−D2000, also indicates that the incorporated silicate network is also helpful for the suppression of D2000 crystallization.

Crystallinity. Mobility within the polyether chains depends on at least two parameters: mobility in the amorphous phase, which is grossly characterized by the T_g, and the amount of crystalline phase. The area under the curve for the melting endotherm in DSC data is related to the crystallinity in the specimens. Table 1 also gives the changes in the degree of the crystallinity (χ) of the D2000 host as a function of silica and lithium contents. The degree of crystallinity of the hybrid electrolytes was evaluated from the ratio of the experimentally determined ΔH_f to the heat of fusion of 100% pure D2000 (113 J/g). As seen in Table 1, the D2000 crystallinity in the hybrid electrolyte systems decreases as the salt concentrations and the inorganic components are increased.

FTIR Analysis. Infrared spectroscopy is a convenient method to provide the information about the development of an organic−inorganic network and also can be employed to study the interaction of the polyether with the lithium salt. Figure 2 shows the FTIR spectra of the 0.2−*y*−D2000 hybrid electrolytes with various $LiClO_4$ concentrations. Two major peaks associated with C−O−C symmetric and asymmetric stretching vibrations were observed at 1147 and 1115 cm^{-1} for pure D2000 (Figure 2a). While the silica was incorporated into the polymer matrix, in the absence of lithium salts, these two bands became broader since the characteristic absorption bands of the hydrolysis product of TEOS and GLYMO were also expected to appear in the same region (Figure 2b). The typical absorption band for noncondensed Si−OH was at around 950 cm^{-1}, and typical absorption bands for Si−O−Si network vibrations were at around 1210 and 1075 cm^{-1}.[45,46] With the addition of the lithium salts, two sharp peaks at 1120 and 1110 cm^{-1} appeared, suggesting that the ether group of D2000 had some interactions with the added lithium cations. Although changes in the intensity, shape, and position of the C−O−C stretching mode are associated with the polyether−$LiClO_4$ interactions, the dependence of the absorption peaks of C−O−C on the salt concentrations is not clarified in FTIR spectra in the present case because the absorption peaks of C−O−C overlap with those of Si−O−Si and Si−O−C. A close examination of the spectra indicates that a broad shoulder at ca. 880 cm^{-1} is also present for the hybrids doped with lithium salt, which is the characteristic of the metal−oxygen breathing motion, and evidence for the formation of crown ether complexes between D2000 and Li^+ cation.[45,46]

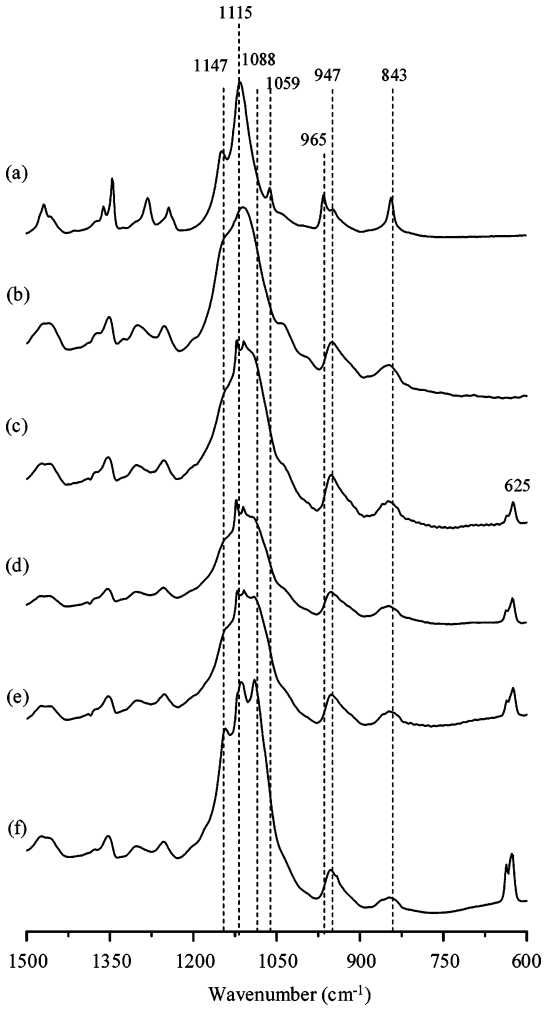

Figure 2. FTIR spectra of (a) pure D2000, (b) 0.2−∞−D2000, (c) 0.2−32−D2000, (d) 0.2−24−D2000, (e) 0.2−16−D2000, and (f) 0.2−8−D2000 in the region of 1500−600 cm^{-1}.

Table 2. Conductivity, Lithium Diffusion Coefficient, and FTIR Deconvolution Results of the 0.2−*y*−D2000 Hybrid Electrolytes Studied

	30 °C		60 °C		
y, [O]/[Li]	σ, S/cm	D_{Li}, cm^2/s	σ, S/cm	D_{Li}, cm^2/s	IR, free ClO_4^-, %
32	6.23×10^{-5}	1.14×10^{-7}	3.13×10^{-4}	2.05×10^{-7}	78.2
24	5.42×10^{-5}	8.27×10^{-8}	2.40×10^{-4}	9.05×10^{-8}	72.2
16	2.06×10^{-5}	5.65×10^{-8}	1.86×10^{-4}	8.82×10^{-8}	71.3
8	6.13×10^{-6}	2.70×10^{-8}	1.11×10^{-4}	6.94×10^{-8}	70.0

Two bands observed at 625 and 635 cm^{-1} due to the vibration modes of ClO_4^- ions are of particular interest.[47−49] The characteristic $\nu(ClO_4^-)$ mode of $LiClO_4$ is particularly sensitive in changing the ion−ion interactions in the electrolyte systems. According to previous literature,[47−49] the band centered at 625 cm^{-1} has been assigned to the vibration of the "free" ClO_4^- anion, which does not interact directly with the lithium cations, and the band centered at 635 cm^{-1} to the vibration of the $Li^+ClO_4^-$ contact−ion pairs. To investigate the behavior of ion association in the present hybrid system, the spectral features of $\nu(ClO_4^-)$ mode were fitted with Gaussian−Lorentzian functions. Table 2 gives the fraction of free cations as a function of salt concentrations for the hybrid electrolytes, in which the fraction is calculated as the ratio of the area under the 625 cm^{-1} mode to the total area under the $\nu(ClO_4^-)$ envelope. As seen in Table 2, the fraction of free anions decreases with increasing

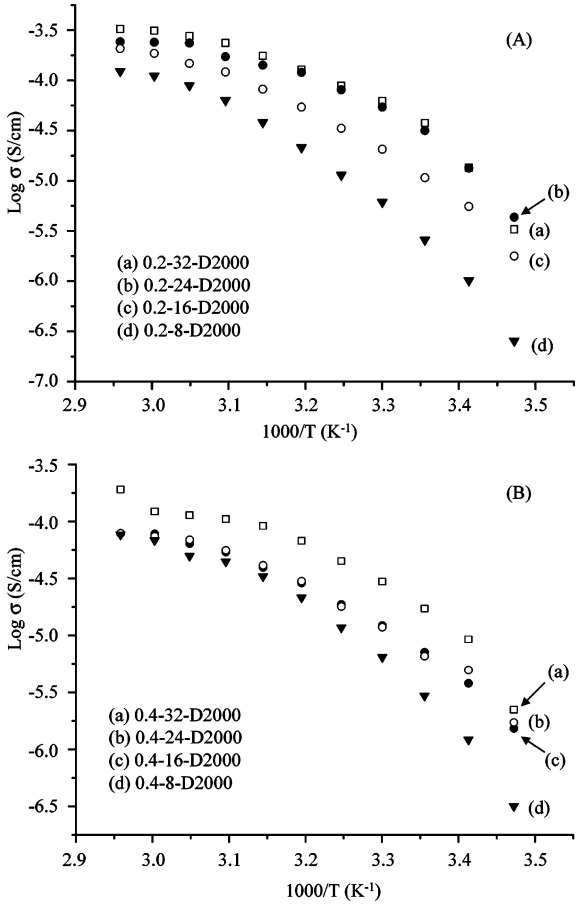

Figure 3. Temperature dependence of ionic conductivity of the hybrid electrolytes studied: (A) 0.2−*y*−D2000 and (B) 0.4−*y*−D2000 with various [O]/[Li] ratios.

salt concentrations. About 78% of ClO_4^- exists as spectroscopically free species for 0.2−32−D2000, while only about 70−72% of free ClO_4^- is observed for other electrolytes. Although these numbers are not remarkably different, we can still see a clear difference between 0.2−32−D2000 and other samples, as shown in the 600−650 cm^{-1} range of Figure 2. The PEO/$LiClO_4$ electrolyte has a degree of ionic dissolution of around 70% when the [O]/[Li] ratio is larger than 8.[50] It has been shown that the addition of an inorganic component like α-Al_2O_3 can significantly increase the degree of ionic dissolution to above 80%.[50b] Given that PPO is expected to have a poorer ability to dissolve salts as compared to PEO, our hybrid systems based on the polymer D2000 have a high degree of ionic dissolution, suggesting that the effect of the silica network resulting from the sol−gel condensation of silica precursors is substantial as in the case of composite polymer electrolytes.

Ionic Conductivity. Figure 3 shows the effects of $LiClO_4$ concentration, silica content, and temperature on the ionic conductivity (σ) of the hybrid electrolytes. As seen in Figure 3, it is clear that the temperature dependence of the conductivity is not linear. The variation of conductivity with temperatures follows the VTF (Vogel−Tamman−Fulcher)-like relationship, indicating that the ion mobility is coupled with the segmental motion of the polymer chain. The 0.2−32−D2000 hybrid exhibits the highest ionic conductivity values of 6.23×10^{-5} S/cm at 30 °C and 3.13×10^{-4} S/cm at 60 °C (Table 2). With increasing salt concentration, on the other hand, the ionic conductivity remarkably decreases, especially for the hybrid electrolyte with the largest amount of the lithium salt (i.e., [O]/[Li] = 8). An increase of the inorganic component fraction also decreases the conductivity of the material for a given [O]/[Li] ratio. For example, the 0.4−32−D2000 sample only exhibits a conductivity value of 2.97×10^{-5} S/cm at 30 °C, which is about two times lower than that of 0.2−32−D2000. To some extent, this is expected given that the larger contents of the silicate network must have a certain blocking effect on long-range ion transport, making the remaining conduction pathways more tortuous.

Despite extensive research efforts, the best conductivities reported for the solid EO-based polymer electrolyte systems with various modifications reach $(2-5) \times 10^{-5}$ S/cm at room temperature. Two types of organic−inorganic hybrid electrolytes, depending on the connection between the inorganic (siloxane) and organic (polymer) phases, have been reported in the literature.[15,18−20] In class I materials, organic and inorganic components were linked through weak physical bonds such as hydrogen bridges or van der Waals bonds. In class II hybrids, there are covalent bonds between the inorganic and organic phases. Although the class I hybrids have higher room-temperature ionic conductivities (up to 10^{-4} S/cm) than the class II hybrids, the type I hybrids have much lower chemical stabilities. The present hybrid belongs to type II hybrids but with higher ionic conductivity (6.2×10^{-5} S/cm at 30 °C), which is markedly high as compared to most of the organic−inorganic hybrids reported in the literature.[22,23,27] Moreover, the room-temperature conductivity value of our present hybrid electrolytes is at least 2 orders of magnitude higher than that of the PEO-based electrolytes and is also comparable to the highest conductivity values reported for most of the polymer electrolytes with various modifications. Although some novel approaches for PEO modifications such as grafting, block copolymerization, and cross-linking are promising, the fact that their preparation requires nontrivial synthetic processes is a serious drawback for practical application. The advantages of the present hybrid electrolytes are that they can be easily prepared and also have an excellent mechanical stability, due to the silica network incorporating into the polymer bulk, and high ionic conductivity.

The factors governing the conductivity need further discussion. The less crystalline 0.2−8−D2000 and 0.4−8−D2000 samples exhibit the lowest conductivity. This is in contrast to the concept that more amorphous characteristics of the polymer are more favorable for the ion transport in the conventional SPEs. Thus, the amorphous characteristic of the polymer is not the dominating factor governing the ion transport in the present case. The comparison of DSC and conductivity data for all the samples studied shows that there is no obvious dependence of the crystalline phase fraction and conductivity. By contrast, the T_g and the conductivity are more closely connected.

It is generally accepted that ionic conductivity in polymer electrolytes is mainly attributed to a property of amorphous phase above their glass transition temperatures. The conductivity varies with a wide range of factors, such as cation and anion types, salt concentration, and temperature, etc. To design effective SPEs, two opposite effects on the ionic transport properties must be thoroughly understood, namely, the increase in the number of charge carriers and the decrease in free volume.[51] The conductivity of a homogeneous polymer electrolyte phase may be given as

$$\sigma(T) = \sum^{i} n_i q_i \mu_i \qquad (2)$$

where n_i is the number of charge carriers, q_i is the charge on each charge carrier, and μ_i is the mobility of charge carriers.

Scheme 1. Schematic Representation of the Present Hybrid System

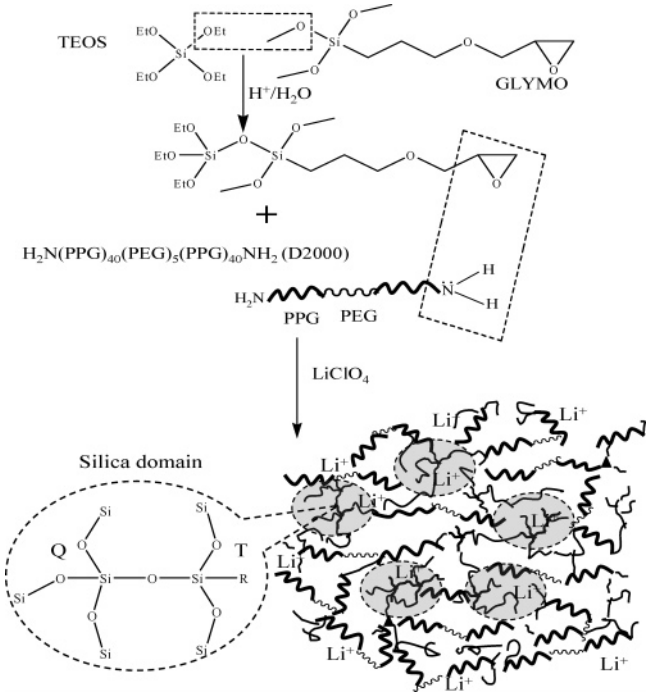

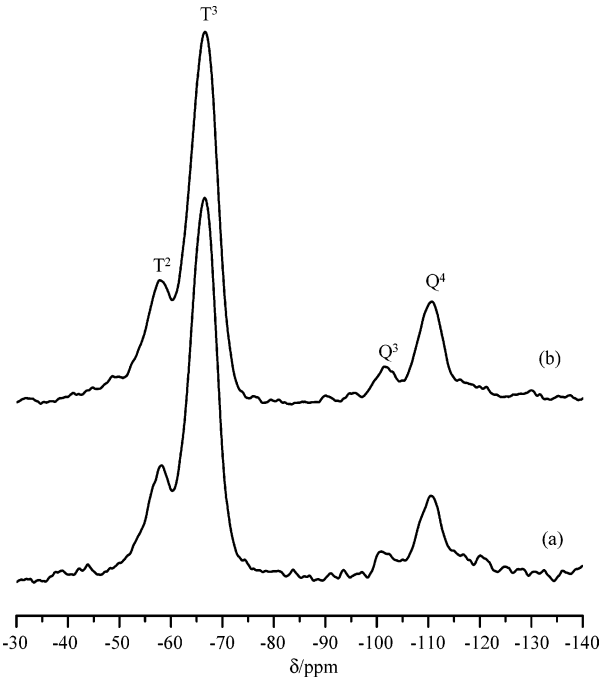

Figure 4. ^{29}Si MAS NMR spectra of (a) 0.4−32−D2000 and (b) 0.4−8−D2000.

According to eq 2, the ionic conductivity depends on the amount of charge carriers in the system and the mobility of the various species. As the salt concentration is increased, the number of charge carriers is increased, but the average free volume is decreased as indicated from the increase in T_g due to the interaction of Li^+ with ether oxygens, which partially interrupts the local motion of the polymer segment via the formation of transient cross-links. The decrease in segmental mobility arising from transition cross-linking and the increase of ionic association leading to the formation of ion pairs or aggregates are verified by DSC and FTIR, respectively. At a relatively high $LiClO_4$ concentration, the formation of ion pairs or aggregates decreases the number density of charge carriers present. These aggregates naturally contribute less effectively to charge transport and eventually hinder the mobility of the charge carriers throughout the polymer matrix. Moreover, the formation of transient ion−polymer cross-links would be expected to restrict segmental mobility and therefore reduce conductivity. Both effects result in a reduction in bulk ionic conductivity at high salt concentrations.

On the basis of the effective medium theory, Wieczorek et al. have suggested a qualitative model, which includes the presence of a more conductive space charge interphase between the polymer electrolyte and filler particles for composite polymer electrolytes.[52] It has been reported that the number of ions available for conduction is not the leading cause for the increase in conductivity exhibited in amorphous and semicrystalline host polymer. Instead, the increase in conductivity is due to the influence of the filler on the mobility of both the polymer and the salt.[53] The model relates the conductivity enhancement to the existence of a space−charge layer at the electrolyte/filler interface. According to the model, the present hybrid electrolyte can be treated as a two-phase system consisting of a polymer ionically conducting matrix with dispersed silica network, as illustrated in Scheme 1. At low salt concentration levels, the extent of contact ion pairs is low and the conductivity is dominated by the mobility of charge carriers, which is promoted by the existence of a space−charge layer at the polymer/silica interface. This can be further supported by the diffusion constant measurements of lithium cations.

^{29}Si MAS NMR. Solid-state ^{29}Si NMR measurements were performed in order to determine the structure of the silicate networks. Four major signals at −101 and −110 ppm, corresponding to Q^3 ($Si(OSi)_3(OH)$) and Q^4 ($Si(OSi)_4$) sites, and at around −65 and −55 ppm, corresponding to T^3 ($RSi(OSi)_3(OH)$, R = alkyl group) and T^2 ($RSi(OSi)_2(OH)_2$) sites, were observed for the two selected 0.4−32−D2000 and 0.4−8−D2000 samples (Figure 4). The observation of T groups indicates the presence of organosilane groups in the materials. The spectral features for both samples are basically the same, indicating that the condensation of the silicate network is not affected by different [O]/[Li] ratios. From these normalized peak areas, the ratios of $T^m/(T^m + Q^n)$ are in close agreement with those expected on the basis of the composition of the initial mixture.

^{13}C CP/MAS NMR. While calorimetric experiments help assess the global dynamics of the material, solid-state ^{13}C CP/MAS NMR experiments performed with various contact times are useful to gain more insights into the influence of Li^+ ions on the polymer chain dynamics.[36] Figure 5 shows the ^{13}C CP/MAS NMR spectra of the hybrid electrolytes acquired at a short contact time of 1.2 ms. The dominant peak at 70.6 ppm is assigned to methylene carbons adjacent to ether oxygens of the polymer chains, and the peak at 17.3 ppm is due to the CH_3 groups of PPG chains. New peaks at 22.9 and 8.7 ppm are clearly visible when the silica is incorporated and are assigned to the methylene carbons in the α and β positions to the silicon atom, respectively, due to GLYMO. The ^{13}C peaks at 44 and 51 ppm expected for the carbon atoms in the epoxide ring of GLYMO are also observed, indicative of the incompleteness of the epoxide ring opening. Besides the major peak at 70.6 ppm, there are some peaks at ca. 73.1 and 74.9 ppm that are also clearly resolved for 0.4−∞−D2000 and 0.4−32−D2000. These peaks become a broader shoulder and are no longer resolved at high levels of salt doping. Some broader shoulders at ca. 60−65 ppm are also observed. Based on its relatively low intensity, the peak of 73.1 ppm can be assigned to the

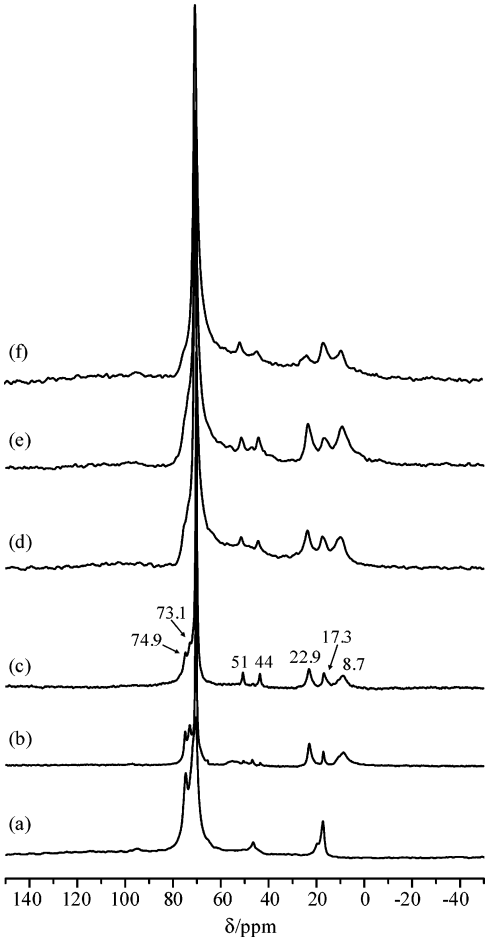

Figure 5. ^{13}C CP/MAS NMR spectra of (a) pure D2000, (b) 0.4−∞−D2000, (c) 0.4−32−D2000, (d) 0.4−24−D2000, (e) 0.4−16−D2000, and (f) 0.4−8−D2000, acquired with a contact time of 1.2 ms.

Table 3. ^{13}C CP/MAS NMR Results of the 0.4−*y*−D2000 Hybrids Studied

		70.6 ppm	
sample	*y*, [O]/[Li]	T_{CH}, ms	$T_1\rho$(H), ms
0.4−*y*−D200 0	32	2.15	800
	24	1.35	274
	16	1.28	43
	8	0.46	32

carbon attached to ether oxygens of GLYMO, while the peaks at around 74.9 and 60−65 ppm are due to the formation of methyl ether terminal groups and diol function from the polymerization reaction of GLYMO.[54] The peaks in the 72−75 ppm region may also result from the -OCH_2 groups of the PEG and PPG segments at chain ends. The high level of salt doping causes a more broad distribution of the environments of the polymer chains, which results in a broader low-field shoulder near the peak at 70.6 ppm (Figure 5d−f).

Due to the complex environments in the region of 72−75 ppm, we focused on the ^{13}C CP signal intensity for the ether carbon at 70.6 ppm as a function of contact times and salt doping levels. The results of the contact time measurements for the peak at 70.6 ppm are presented in Table 3. The T_{CH} and $T_1\rho$-(H) measurements were obtained by fitting the CP signal intensities with the following formula:[55]

$$M(t) = M_0 \exp(-t/T_1\rho(\mathrm{H}))(1 - \exp(-t/T_{CH})) \qquad (3)$$

where $M(t)$ is the peak intensity as a function of contact time t, M_0 is the normalization constant, $T_1\rho$(H) is the proton spin−lattice relaxation in the rotating frame, and T_{CH} is the cross-polarization time constant. Since CP is a measure of the efficiency of magnetization transfer by the dipolar coupling from ^{1}H to ^{13}C, the CP time constant (T_{CH}) derived from variable contact time measurements can give quantitative descriptions of cross-polarization and relaxation behavior. Since cross-polarization is most efficient for the static ^{1}H−^{13}C dipolar interactions, the less mobile carbon groups exhibit the faster cross-polarization rate or the shorter T_{CH}. As seen in Table 3, the -OCH_2 groups (70.6 ppm) exhibit T_{CH} values of 2.15 and 0.46 ms and $T_1\rho$(H) values of 800 and 32 ms for 0.4−32−D-2000 and 0.4−8−D2000, respectively. The slower growth in spin magnetization for the peak at 70.6 ppm for 0.4−32−D2000 reflects that the rapid motion of 0.4−32−D2000 makes the CP signal transfer from the proton spins less efficient than for 0.4−8−D2000. The significant decrease in T_{CH} for the peak at 70.6 ppm with increasing salt concentrations also suggests a possible coordination of Li^+ ions with the ether oxygen atoms of the polymer chain, thereby restricting the segmental motion of the polymer chains.

Domain Size. From the analysis of CP signals due to the silica domain (22.9 and 8.7 ppm) as a function of contact time, it is also clear that there are distinct proton spin reservoirs coupled to the different carbons since the $T_1\rho$(H) values obtained for the polymer and silica domains are different. This indicates that proton spin diffusion is relatively slow due to the phase separation in the hybrid electrolytes. The $T_1\rho$(H) value for the peak at 70.6 ppm drops as the salt concentration is increased, reflecting that proton−proton spin diffusion becomes more efficient due to the increased proton−proton dipolar interaction. This observation indicates that the coordination between Li^+ ions and the polyether chains effectively reduces the chain motion, resulting in the chain rigidity, and therefore increases proton−proton dipolar interaction.

It has been demonstrated that measurements of $T_1\rho$(H) relaxation time can be used to obtain the domain size in polymers.[56] Diffusion of ^{1}H magnetization within the hybrid system tends to average the ^{1}H relaxation time and to lead to an averaging effect on the $T_1\rho$(H) of the different components. In a homogeneous system, a single spin−lattice relaxation time is usually observed. For a heterogeneous system like the present case, more than one $T_1\rho$(H) value are often found because there is insufficient time for spin diffusion to equilibrate the magnetization in the different phases. Therefore, $T_1\rho$(H) relaxation time can provide an estimate of the diffusive path length and hence the sizes of heterogeneities of the hybrid. A useful approximate estimation of the domain size is given by relating the spin diffusion and the relaxation time as follows:[56]

$$\langle L \rangle = (6D_{\mathrm{H}}T)^{1/2} \qquad (4)$$

where $\langle L \rangle$ is the average diffusive path length for the effective spin diffusion, D_H is the proton spin diffusion coefficient determined by the average proton−proton distance and the strength of the dipolar interaction, and T is the characteristic time over which the spin diffusion proceeds. The organic and inorganic phases, namely, polymer- and silica-rich phases, in the present hybrid electrolytes are from two independent domains where the domain size is smaller than the maximum diffusive path length of proton spin diffusion over a $T_1\rho$(H) relaxation time. Assuming the proton diffusion constants are the same, the polymer-rich domain of 0.4−32−D2000 is more homogeneous in a scale larger than 0.4−8−D2000 since the former has a larger $T_1\rho$(H) value.

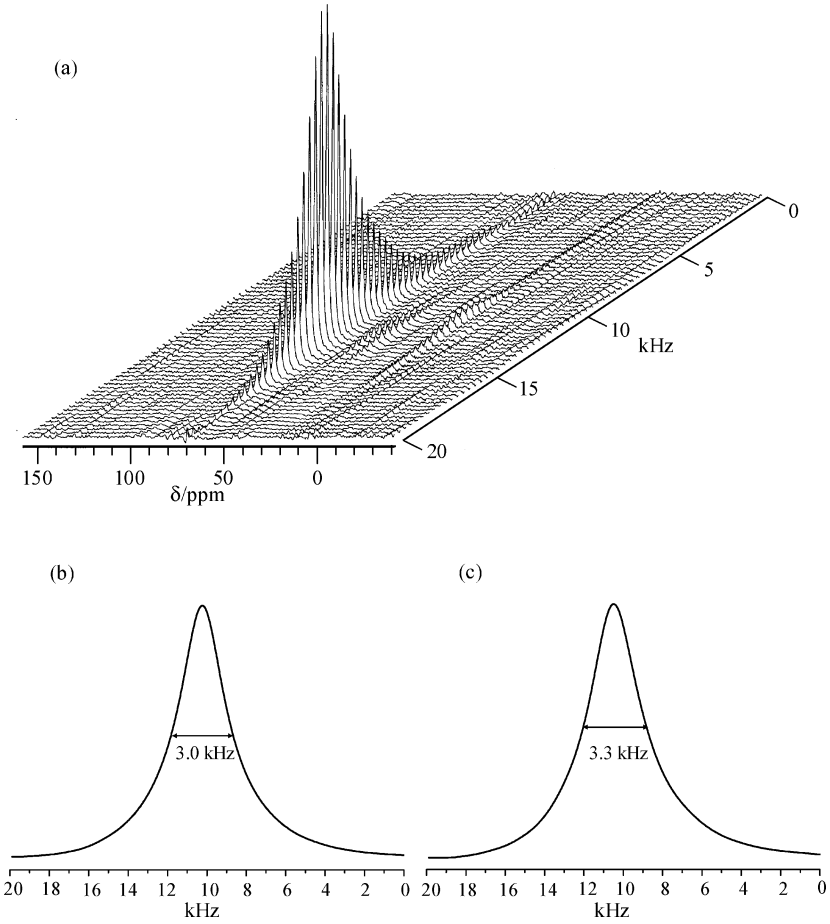

Figure 6. (a) 2D $^{1}H-^{13}C$ WISE spectrum for 0.4−32−D2000 and the projections of the ^{1}H dimension of the peak at 70.6 ppm for (b) 0.4−32−D2000 and (c) 0.4−8−D2000.

2D $^{1}H-^{13}C$ WISE NMR. 2D WISE NMR has been widely used for determining dynamic heterogeneities in solid polymers.[43] By means of 2D WISE NMR, the spectroscopic information about the dynamic behavior within a system can be qualitatively assessed by examining the proton line shapes that are directly related to structural elements resolved in the ^{13}C CP/MAS NMR spectrum. Therefore, 2D WISE NMR spectroscopy is used here to further quantify chain mobility in order to confirm the results obtained from the CP time constant T_{CH} measurements. Therefore, a deeper insight into the effect of the addition of salt on the chain mobility associated with a specific segment can be revealed.

For convenience to make a comparison, Figure 6 shows the projections of the ^{1}H dimension of the WISE spectra associated with the 70.6 ppm peak for 0.4−32−D2000 and 0.4−8−D2000. The line width of the ^{1}H line reflects the nature of the dipolar interaction between the protons and thus can be used to monitor the mobility of polymer chains. For the selected carbon at 70.6 ppm, the 0.4−8−D2000 sample exhibited a larger line width (3.3 kHz) in the ^{1}H dimension than the 0.4−8−D2000 sample (3.0 kHz). This reflects some microscopically dynamic changes of the polymer chains as the salt concentration is increased. Thus, the 2D WISE spectra further confirms our earlier conclusion that the mobility of the polymer chains decreases as the salt content is increased due to complexation of lithium cations with the ether oxygen atoms. In comparison to most crystalline or semicrystalline polymers, which always exhibit a proton line width larger than 50 kHz, the much narrower proton line width from the 2D WISE NMR reveals considerable chain mobility for the present hybrid electrolytes.

^{7}Li Line Width Measurements. The static ^{7}Li line width measurements as a function of temperature are useful in determining the status of the motional narrowing process of the lithium cations. The temperature dependence of the static ^{7}Li line width for the 0.2−8−D2000 and 0.4−8−D2000 samples, as shown in Figure 7, can be described by a curve composed of two plateaus separated by a temperature range where a rapid change in the line widths occurs. In the low-temperature region of −140 to −30 °C, below the T_g of the systems, the line widths are very broad (fwhh = ∼6 kHz) and are not very sensitive to temperature changes. This suggests that the lithium ions are not mobile at low temperatures and thus are not conductive as evidenced from conductivity measurements. The broad line width observed is the result of increased quadrupolar and/or internuclear dipole−dipole interactions. Upon increasing the sample temperature, the line widths are motionally narrowed, with the onset of narrowing correlating with the T_g. Motional narrowing begins when the rate of the fluctuations ($1/\tau_c$) of either the local dipolar fields or the electric field gradients (EFG) is comparable to their respective rigid lattice line widths (Δ_{RL}) or when $1/\tau_c \sim \Delta_{RL}$, where τ_c is the motional correlation time.[57] This observation is also consistent with the NMR behavior observed in traditional polyether-based polymer electrolytes, which only show motional narrowing of the ^{7}Li line width once the T_g is exceeded. This implies that the mobility of cations appears to be closely associated with the segmental motions of the polymer above the glass temperature. This phenomenon is corroborated by the VTF-like behavior in conductivity.

Narrowing of the NMR line commences when the rate of the local field fluctuations is comparable to the rigid lattice line

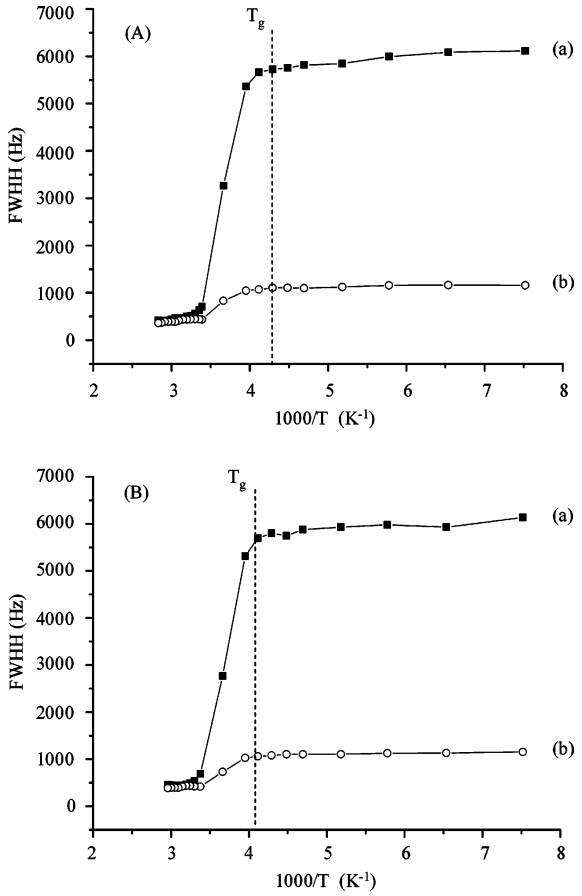

Figure 7. ^{7}Li static line widths of (A) 0.2−8−D2000 and (B) 0.4−8−D2000 measured (a) without and (b) with proton decoupling as a function of temperature.

width of about 6 kHz. At sufficiently high temperatures, each sample exhibits a common high-temperature line width limit of about 0.5 kHz. The similarity in the temperature dependence of the line width for each sample indicates that a common diffusion mechanism and similar ^{7}Li local environments exist for all the samples studied. This suggests that the ions segregate into regions of high density (polymer-rich domain) and low density (silica-rich domain), which is also evidenced by ^{7}Li MAS NMR measurements as shown below. The change with salt concentration is only associated with the percentages of the two kinds of regions (Scheme 1). A significant reduction in the ^{7}Li line width (from 6.0 to 1.0 kHz) in the low-temperature region (i.e., from −140 to −30 °C) is achieved by the use of the decoupling techniques, which effectively removes the ^{1}H−^{7}Li dipolar interactions of the lithium cation and the polymer backbone. The ^{1}H−^{7}Li dipolar coupling accounts for about 85% reduction in the ^{7}Li line widths, comparable to a 90% reduction observed in PEO_8LiClO_4.[58] Moreover, the line associated with the central transition ($+^1/_2 \leftrightarrow -^1/_2$) is not broadened (up to first-order) by the ^{7}Li quadrupole coupling. The central line broadening due to the second-order quadrupole interactions is expected to be small since its estimated contribution is on the order of hertz.[57] Therefore, the ^{1}H−^{7}Li dipolar interaction is predominately responsible for the temperature behavior of the ^{7}Li line widths.

The information on the nuclear interactions can be obtained by analyzing the second moment (M_2) of the NMR signal. While in crystals M_2 can be easily obtained by the Van Vleck formalism,[59] in the case of amorphous phases an experimental estimate of the second moment can be obtained by the relationship[60]

$$M_2 = 0.721(^1/_2\Delta H_{1/2})^2 \quad (5)$$

where $\Delta H_{1/2}$ is the fwhh expressed in gauss. According to eq 5, it follows that the ^{7}Li second moment values are ∼2.36 G^2 for all the samples studied. Besides the ^{1}H−^{7}Li dipolar broadening of the ^{7}Li central line, there are other heteronuclear contributions from the coupling with ClO_4^- species and polymer chains. Given the small gyromagnetic factors and/or low natural abundance of ^{13}C, ^{35}Cl, and ^{17}O stable isotropes, one can conclude that the residual line width of 1.0 kHz in the proton-decoupled ^{7}Li static NMR spectra is mainly due to the ^{7}Li−^{7}Li homonuclear interaction. Therefore, the ^{7}Li second moment contains the following dipolar contributions:

$$M_2(^7\text{Li}) = M_2(^7\text{Li}-^7\text{Li}) + M_2(^7\text{Li}-^1\text{H}) \quad (6)$$

The average ^{7}Li−^{7}Li distance can be estimated to be close to 5 Å for the present hybrid electrolytes, which is the same order of the average distance between two consecutive ether oxygens in the PEO chain (∼3 Å) and also in good agreement with the findings of Wintersgill et al., who reported an average ^{7}Li−^{7}Li separation of 4.7 Å in PVAc:$LiClO_4$ = 8:1.[61]

Li T_1 Measurements. Information about the local environment and dynamics of the lithium cations may be obtained from measurements of the spin−lattice relaxation time (T_1). Relaxation time T_1 measurements are sensitive to fluctuations in the local environment on a time scale comparable to the inverse of the NMR resonance frequency, i.e., nanoseconds. In general, in the case of quadrupolar nucleus ^{7}Li ($I = ^3/_2$), the spin−lattice relaxation should be described by a superposition of two or more exponentials.[59] Due to the small quadrupole moment of ^{7}Li, however, deviations from a single-exponential function are often difficult to detect as was also found in the present study. For all samples and temperatures, the ^{7}Li T_1 data were calculated using only one exponential function.

^{7}Li spin−lattice time (T_1) measurements were performed to analyze the lithium ion transport behavior over the temperature range of −60 to +80 °C, as shown in Figure 8. T_1 decreased drastically as the sample temperature was increased, suggesting that the lithium ions became more and more mobile. No obvious T_1 minima were observed. This is in contrast to the well-known phenomenon often reported in PEO−salt complexes. Another important feature is that 0.2−32−D2000 exhibits a smaller T_1 value than 0.2−8−D2000 and 0.4−8−D2000 in the temperature range studied. These results indicate that the relative mobility of the Li^+ ions in the 0.2−32−D2000 sample is higher than other samples, which agrees with the conductivity data. Because the T_1 minimum occurs when the motional correlation time is comparable to the reciprocal of the Larmor frequency of the ^{7}Li nucleus, the absence of a well-defined T_1 minimum implies a broad distribution of correlation times, indicative of structural heterogeneity of the lithium cations. The heterogeneity of Li^+ local environment can be further confirmed by the proton-decoupled ^{7}Li MAS NMR (Figure 9). Therefore, the relaxation processes observed in the present hybrid electrolytes cannot be described in terms of the simple Bloembergen−Purcell−Pound (BPP) model,[62] which is generally valid for the homogeneous spin system with a single correlation time. More sophisticated analyses of the spin−lattice relaxation behaviors have been proposed to obtain information on the spin dynamics and, therefore, on the site distribution.[63] However, these methods are hardly applicable to complex multiphase systems such as the present case.

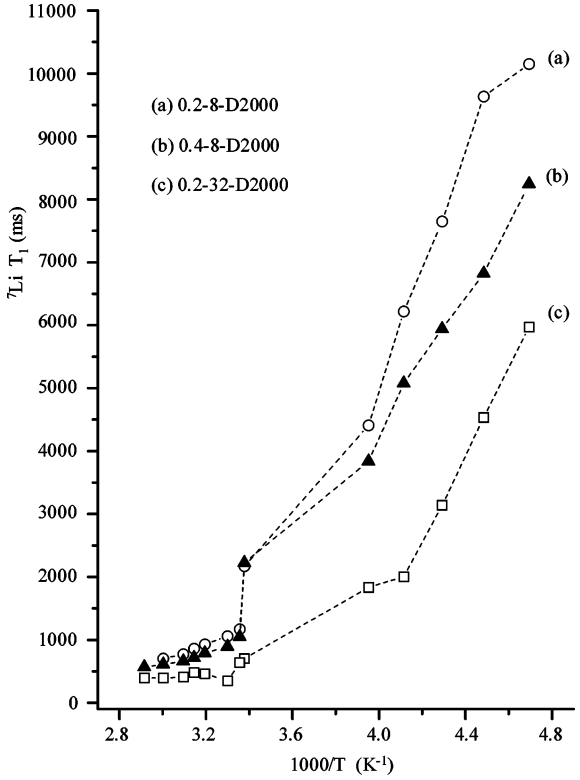

Figure 8. ^{7}Li T_1 values of (a) 0.2−8−D2000, (b) 0.4−8−D2000, and (c) 0.2−32−D2000 as a function of temperature.

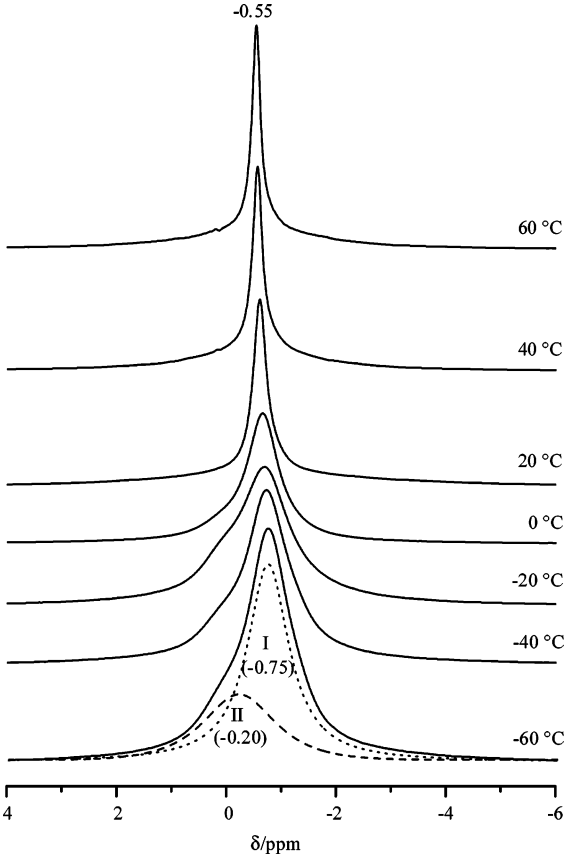

Figure 9. Variable-temperature ^{7}Li{^{1}H} MAS NMR spectra of 0.2−8−D2000, acquired at a spinning speed of 3 kHz.

Proton-Decoupled ^{7}Li MAS NMR. Variable-temperature ^{7}Li{^{1}H} (i.e., proton-decoupled) MAS NMR measurements were performed to probe the local environments of the Li^+ cation. At −60 °C, the ^{7}Li resonance at −0.75 ppm (site I) associated with a shoulder at about −0.20 ppm (site II), with an intensity ratio of 0.77:0.23 (site I:site II), were observed for 0.2−8−D2000 (Figure 9), indicating that there are two distinct ^{7}Li local environments present in the hybrid electrolytes. Upon raising the sample temperature to above 20 °C, these two sites merged together into a peak at −0.55 ppm. Site I with a larger intensity is assigned to the lithium cation in the polyether domain. As the content of silica is doubled, the fraction of site II increases from 0.23 for 0.2−8−D2000 to 0.39 for 0.4−8−D2000. On the basis of the fact that its intensity increases with increasing the silica content, site II is assigned to the lithium cation in the polymer−silica interface and/or in a silica-rich domain. The present NMR observation shows that variable-temperature ^{7}Li-{^{1}H} MAS NMR technique is able to resolve the different lithium local environments present in the hybrid system due to the presence of microphase-separated structures. The different local environments of the lithium cations also correlated well with the complex T_1 behaviors.

Without incorporation of silica, it is impossible to form a stable free-standing film just by adding the lithium salt. This is also an indication that the polymer phase is chemically connected and segregates to the interpenetrating silica network. Therefore, the hybrid can be viewed as a microscopic two-phase system composed of dispersed siloxane nanocluster, chemically cross-linked with -NH_2 groups at the end of the polymeric chain. As a result, the ^{7}Li cations can exist in both the polymer-rich and silica-rich domains, as illustrated in Scheme 1.

Diffusion and Ionic Conductivity. As demonstrated above, the heterogeneous nature of the present hybrid system complicates the detailed analysis of NMR relaxation times. A more direct NMR method for measuring the ion mobility is PGSE NMR techniques. The most important advantage of the PGSE NMR method over NMR relaxation-based techniques is the direct measurement of diffusion constants (D) of the charged carriers without any assumptions. Since the self-diffusion coefficients measured by the PGSE NMR method include all the species (i.e., isolated and ion-paired), the measured values are the population-weighted averages of the various states. The ^{7}Li diffusion coefficients for the 0.2−y−D2000 samples were measured as a function of temperature, in the range of 30−120 °C, and the representative diffusion curves of 0.2−16−D-2000 as a function of temperature are shown in Figure 10. As shown in Figure 11, the increase in the ^{7}Li diffusion coefficient is more pronounced at elevated temperatures. The plots are not linear for the whole temperature range investigated, suggesting the diffusion process is quite complicated in the present hybrids. Since the ^{7}Li diffusion coefficient is a mean value for all Li species, the decrease in ^{7}Li diffusion coefficients with increasing salt concentrations could be due to a change in the formation of ion pairs, as demonstrated by FTIR.

Conductivity and ionic diffusion are commonly related by the modified Nernst−Einstein equation:

$$\sigma_{calc} = Nq^2(D_{Li} + D_{anion})\alpha/kT \qquad (7)$$

where σ_{calc} is the calculated ionic conductivity, N is the number of ions per unit volume, q is the charge of the ions, α is the degree of ion dissociation, and D_{Li} and D_{anion} are the diffusion coefficients of the cation and anion, respectively. Commonly, the calculated conductivity with the measured self-diffusion coefficients of the fluorine-containing anions D_F and the cations D_{Li} (determined by pulsed field gradient NMR) is larger than experimentally observed conductivity.[39−42,64] Since the diffusion

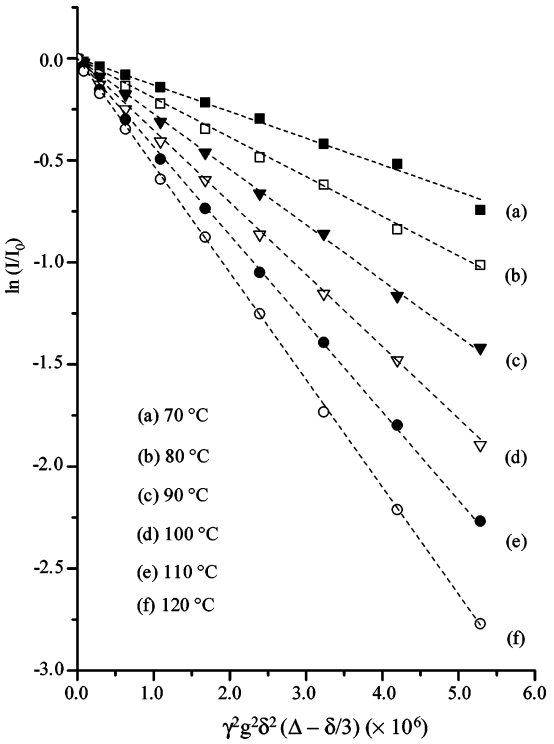

Figure 10. Representative diffusion curves of 0.2−16−D2000 as a function of temperature.

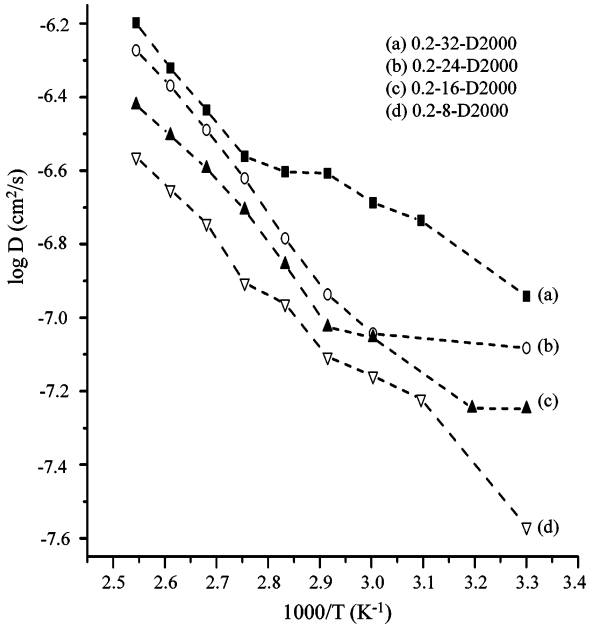

Figure 11. ^{7}Li diffusion coefficients of 0.2−y−D2000 as a function of temperature.

constant of the anion (ClO_4^-) is unknown in the present study, we cannot accurately calculate the percentages of the conductance that are associated with the cations and the anions, respectively. As seen in Table 2, however, a clear correlation between the mobility of the lithium cation and the ionic conductivity can be made. Although the carrier numbers are larger in 0.2−8−D2000, the diffusion coefficient of the lithium cation in 0.2−8−D2000 is smaller compared to those of other compositions in 0.2−y−D2000. Thus the total conductivity is low for 0.2−8−D2000. By contrast, the 0.2−32−D2000 sample with the lowest salt concentration exhibits the highest cation diffusion constant over the temperature range investigated (Figure 11). This explains why the 0.2−32−D2000 sample exhibits high conductivity values even with a less amount of lithium cations. At high salt content either phase separation or complex formation might occur to inhibit the ion transport process. Therefore, the mobility of the lithium cations is very decisive for the high conductivity of the present hybrid electrolytes.

It is instructive to compare the conductivity values with the cation diffusion coefficients measured at different temperatures (Table 2). When the temperature was increased from 30 to 60 °C, the conductivity was increased much more than the increase in the D_{Li} values. It has been reported that transport of ions is connected with the segmental motions of polymer chains and ionic transport is predominantly due to ClO_4^- anions at temperatures higher than $1.3T_g$.[65,66] The mechanism for the transport of anions is generally expected to be different from the transport of cations because of the much weaker interactions between the anions and the polymer chains. A faster diffusion of the anions compared with the cations has been observed for similar systems, despite the fact that in all these cases the anions are bigger than the cations. One reason for the enhanced diffusion of the anions could be the increase of the free volume with increasing temperature, allowing the anions to move more freely and therefore faster. The contribution of the diffusion constants of the anion to the total conductivity for the present hybrid electrolytes is therefore significant. The diffusion coefficient of the anions is needed in order to fully understand the present system; new investigations are thus underway, using a lithium salt with fluorine-containing anion such as lithium triflate.

Conclusions

The effect of lithium salt concentrations and silica contents on conductivity, ion structure and dynamics has been investigated in the organic−inorganic hybrid electrolytes based on D2000 complexed with $LiClO_4$ via the co-condensation of GLYMO and TEOS. Specific interactions among ions and polymer matrix have been examined in detail by ^{13}C CP/MAS and 2D WISE NMR experiments; both demonstrate that the segmental mobility of the polymer matrix is affected by the salt concentration. The combined results of conductivity and PGSE NMR self-diffusion coefficient measurements reveal that the conductivity enhancement at low salt concentrations is mainly caused by the high mobility of the lithium cations. The present hybrid electrolytes have an excellent mechanical stability and remarkable high ionic conductivity at room temperature. These important and unique properties make these hybrid electrolytes of definite interest for the development of advanced rechargeable lithium batteries.

Acknowledgment. The financial support of this work by the National Science Council of Taiwan is gratefully acknowledged.

References and Notes

(1) Fenton, B. E.; Parker, J. M.; Wright, P. V. *Polymer* **1973**, *14*, 589.
(2) Vincent, C. A.; Scrosati, B. *Modern Batteries: An Introduction to Electrochemical Power Sources*; Butterworth-Heinemann: London, 1997.
(3) Gary, F. M. *Solid Polymer Electrolytes: Fundamentals and Technological Applications*; VCH: New York, 1991.
(4) Berthier, C.; Gorecki, W.; Minier, M.; Armand, M. B.; Chabagno, J. M.; Rigand, P. *Solid State Ionics* **1983**, *11*, 91.
(5) MacGlashan, G. S.; Andreev, Y. G.; Bruce, P. G. *Nature* **1999**, *398*, 792.
(6) Chung, S. H.; Wang, Y.; Greenbaum, S. G.; Golodnitsky, D.; Peled, E. *Electrochem. Solid-State Lett.* **1999**, *2*, 553.

(7) Golodnitsky, D.; Livshits, E.; Rosenberg, Y.; Lapides, I.; Peled, E. *Solid State Ionics* **2002**, *147*, 265.
(8) Golodnitsky, D.; Livshits, E.; Kovarsky, R.; Peled, E. *Electrochem. Solid-State Lett.* **2004**, *7*, A412.
(9) Croce, F.; Appetechi, G. B.; Persi, L.; Scrosati, B. *Nature* **1998**, *394*, 456.
(10) Croce, F.; Persi, L.; Ronci, F.; Scrosati, B. *Solid State Ionics* **2000**, *135*, 47.
(11) Forsyth, M.; MacFarlane, D. R.; Best, A.; Adebahr, J.; Jacobsson, P.; Hill, A. J. *Solid State Ionics* **2000**, *147*, 203.
(12) Bujdak, J.; Hackett, E.; Ginndis, E. P. *Chem. Mater.* **2000**, *12*, 2168.
(13) Vaia, R. A.; Vasudavan, S.; Krawiec, W.; Scanlon, L. G.; Giannelis, E. P. *Adv. Mater.* **1995**, *7*, 154.
(14) Wong, S.; Zax, D. B. *Electrochim. Acta* **1997**, *42*, 3513.
(15) Mello, N. C.; Bonagamba, T. J.; Panepucci, H.; Dahmouche, K.; Judeinstein, P.; Aegerter, M. A. *Macromolecules* **2000**, *33*, 1280.
(16) Ravaine, D.; Seminel, A.; Charbouillot, Y.; Vincens, M. *J. Non-Cryst. Solids* **1986**, *82*, 210.
(17) Popall, M.; Durand, H. *Electrochim. Acta* **1992**, *37*, 1593.
(18) Judeinstein, P.; Livage, J.; Zarudianski, A.; Rose, R. *Solid State Ionics* **1998**, *28*−*30*, 1722.
(19) Dahmouche, K.; Atik, M.; Mello, N. C.; Bonagamba, T. J.; Panepucci, H.; Aegerter, M.; Judeinstein, P. *J. Sol-Gel Sci. Technol.* **1997**, *8*, 711.
(20) de Souza, P. H.; Bianchi, R. F.; Dahmouche, K.; Judeinstein, P.; Faria, R. M.; Bonagamba, T. J. *Chem. Mater.* **2001**, *13*, 3685.
(21) de Zea Bermudez, V.; Alcacer, L.; Acosta, J. L.; Morales, E. *Solid State Ionics* **1999**, *116*, 197.
(22) Bronstein, L. M.; Joo, C.; Karlinsey, R.; Ryder, A.; Zwanziger, J. W. *Chem. Mater.* **2001**, *13*, 3678.
(23) Dag, Ö.; Verma, A.; Ozin, G. A.; Kresge, C. T. *J. Mater. Chem.* **1999**, *9*, 1475.
(24) Popall, M.; Andrei, M.; Kappel, J.; Kron, J.; Olma, K.; Olsowski, B. *Electrochim. Acta* **1998**, *10*−*11*, 1155.
(25) Simon, P. F. W.; Ulrich, R.; Spiess, H. W.; Wiesner, U. *Chem. Mater.* **2001**, *13*, 3464.
(26) Kao, H.-M.; Chen, C.-L. *Angew. Chem., Int. Ed.* **2004**, *8*, 980.
(27) Bronstein, L. M.; Karlinsey, R. L.; Ritter, K.; Joo, C. G.; Stein, B.; Zwanziger, J. W. *J. Mater. Chem.* **2004**, *14*, 1812.
(28) Ali, F.; Forsyth, M.; Garcia, M. C.; Smith, M. E.; Strange, J. H. *Solid State Nucl. Magn. Reson.* **1995**, *5*, 217.
(29) Ward, I. M.; Boden, N.; Cruickshank, J.; Leng, S. A. *Electrochim. Acta* **1995**, *40*, 2071.
(30) Stallworth, P. E.; Greenbaum, S. G.; Croce, F.; Slane, S.; Salomon, M. *Electrochim. Acta* **1995**, *40*, 2137.
(31) Forsyth, M.; MacFarlane, D. R.; Meakin, P.; Smith, M. E.; Bastow, T. J. *Electrochim. Acta* **1995**, *40*, 2343.
(32) Forsyth, M.; Garcia, M.; MacFarlane, D. R.; Meakin, P.; Ng, S.; Smith, M. E. *Solid State Ionics* **1996**, *85*, 209.
(33) Yang D.-K.; Zax, D. B. *J. Chem. Phys.* **1999**, *110*, 5325.
(34) Ng, S. T. C.; Forsyth, M.; MacFarlane, D. R.; Garcia, M.; Smith, M. E.; Strange, J. H. *Polymer* **1998**, *39*, 6261.
(35) Forsyth, M.; Jiazeng, S.; MacFarlane, D. R. *Electrochim. Acta* **2000**, *45*, 1237.
(36) Lin, C.-L.; Kao, H.-M.; Wu, R.-R.; Kuo, P.-L. *Macromolecules* **2002**, *35*, 3083.
(37) Stejskal, E. O.; Tanner, J. E. *J. Chem. Phys.* **1965**, *42*, 288.
(38) Price, W. S. *Concepts Magn. Reson.* **1997**, *9*, 299.
(39) Johansson, A.; Gogoll, A.; Tegenfeldt, J. *Polymer* **1996**, *37*, 1387.
(40) Gorecki, W.; Jeannin, M.; Belorizky, E.; Roux, C.; Armand, M. *J. Phys.: Condens. Matter* **1995**, *7*, 6823.
(41) (a) Hayamizu, K.; Aihara, Y.; Price, W. S. *J. Chem. Phys.* **2000**, *113*, 4785. (b) Hayamizu, K.; Aihara, Y.; Price, W. S. *Electrochim. Acta* **2001**, *46*, 1475.
(42) Gorecki, W.; Roux, C.; Clémancey, M.; Armand, M.; Belorizky, E. *ChemPhysChem* **2002**, *7*, 620.
(43) Schmidt-Rohr, K.; Clauss, J.; Spiess, H. W. *Macromolecules* **1992**, *25*, 3272.
(44) Mills, R. *J. Phys. Chem.* **1973**, *77*, 685.
(45) Nandi, M.; Conklin, J. A.; Salvati, L.; Sen, A. *Chem. Mater.* **1991**, *3*, 201.
(46) Babonneau, F.; Dire, S.; Bonhomme-Coury, L.; Livage, J. *Inorganic and Organometallic Polymers. II. Sol*−*Gel Synthesis of Heterometallic Oxo Polymers*; ACS Symposium Series 134; American Chemical Society: Washington, D.C., 1994; Chapter 12.
(47) Papke, B. L.; Ratner, M. A.; Shriver, D. F. *J. Phys. Chem. Solids* **1981**, *42*, 493.
(48) Eschmann, J.; Strasser, J.; Xu, M.; Okamoto, Y.; Eyring, E.; Petrucci, S. *J. Phys. Chem.* **1990**, *94*, 3908.
(49) Kioul, A.; Mascia, L. *J. Non-Cryst. Solids* **1994**, *175*, 169.
(50) (a) Wieczorek, W.; Zalewska, A.; Raducha, D.; Florjańczyk, Z.; Stevens, J. R.; Ferry, A.; Jacobsson, P. *Macromolecules* **1996**, *29*, 143. (b) Wieczorek, W.; Zalewska, A.; Raducha, D.; Florjańczyk, Z.; Stevens, J. R. *J. Phys. Chem. B* **1998**, *102*, 352.
(51) Cohen, M. H.; Turnbull, D. *J. Chem. Phys.* **1959**, *31*, 1164.
(52) Wieczorek, W.; Lipka, P.; Zukowska, G.; Wycislik, H. *J. Phys. Chem. B* 1998, *102*, 6968.
(53) Best, A. S.; Adebahr, J.; Jacobsson, P.; MacFarlane, D. R.; Forsyth, M. *Macromolecules* **2001**, *34*, 4549.
(54) Templin, M.; Wiesner, U.; Spiess, H. W. *Adv. Mater.* **1997**, *9*, 814.
(55) Mehring, M. *Principles of High-Resolution NMR in Solids*, 2nd ed.; Springer-Verlag: New York, 1983.
(56) McBriety, V. J.; Douglass, D. C.; Kwei, T. K. *Macromolecules* **1978**, *11*, 1265.
(57) Chung, S. H.; Jeffrey, K. R.; Stevens, J. R. *J. Chem. Phys.* **1991**, *94*, 1803.
(58) Donoso, J. P.; Bonagamba, T. J.; Panepucci, H. C.; Oliveira, L. N.; Gorecki, W.; Berthier, C.; Armand, M. *J. Chem. Phys.* **1993**, *98*, 10026.
(59) Abragram, A. *The Principles of Nuclear Magnetism*; Clarendon: Oxford, U.K., 1961.
(60) Poole, Ch. *Electron Spin Resonance*, 2nd ed.; Wiley: New York, 1983.
(61) Wintersgill, M. C.; Fontanella, J. J.; Calame, J. P.; Smith, M. K.; Jones, T. B.; Greenbaum, S. G.; Adamic, K. J.; Shetty, A. N.; Anden, C. G. *Solid State Ionics* **1986**, *18/19*, 326.
(62) Bloembergen, N.; Purcell, E. M.; Pound, R. V. *Phys. Rev.* **1948**, *73*, 679.
(63) van der Putten, D.; Diezemann, G.; Fujara, F.; Hartmann, K.; Sillescu, H. *J. Chem. Phys.* **1992**, *96*, 1748.
(64) (a) Williamson, M. J.; Hubbard, H. V. St. A.; Ward, I. M. *Polymer* **1999**, *40*, 7177. (b) Ward, I. M.; Williamson, M. J.; Hubbard, H. V. St. A.; Southall, J. P.; Davies, G. R. *J. Power Sources* **1999**, *81*−*82*, 700.
(65) Wieczorek, W.; Chung, S. H.; Stevens, J. R. *J. Polym. Sci., Part B: Polym. Phys.* 1996, *34*, 2911.
(66) Bruce, P. G. *Solid State Electrochemistry*; Cambridge University Press: Cambridge, U.K., 1995; Chapters 5 and 6.

MA051550Q